Journal of Thermal Analysis and Calorimetry (2025) 150:7519–7528
https://doi.org/10.1007/s10973-025-14178-9

Thermomechanical properties of bionanocomposites based on polycaprolactone and halloysite clay nanotubes

Maria Rosalia Carotenuto[1,2] · Giuseppe Cavallaro[1] · Ileana Chinnici[2] · Giuseppe Lazzara[1] · Stefana Milioto[1]

Received: 2 August 2024 / Accepted: 4 March 2025 / Published online: 12 April 2025

Abstract

Bionanocomposites based on polycaprolactone and halloysite clay nanotubes were prepared by melt blending procedure. The nanofiller content was systematically varied in a wide range (from 5 to 60 mass%). We studied the effect of halloysite Addition on the thermal properties of polycaprolactone by thermogravimetric analysis and differential scanning calorimetry. Both techniques evidenced that the thermal characteristics of the nanocomposites depend on the biopolymer/halloysite composition. We observed that the polymer degradation temperature is not affected by halloysite for concentrations up to 15 mass%, while a further addition of the clay nanotubes generated a decrease of the thermal stability of polycaprolactone. Similar results were detected for the polymer melting enthalpy in agreement with a reduction of the polycaprolactone crystallinity. On the other hand, the melting temperature of the polymer was not influenced by halloysite for all the investigated compositions. We studied the viscoelastic properties of the nanocomposites at variable temperatures by dynamic mechanical analysis. These experiments revealed that the presence of the nanotubes can preserve the elastic component of the polymer within a larger temperature range compared to native polycaprolactone. According to this observation, we can conclude that the addition of halloysite nanotubes to the synthetic and biodegradable polycaprolactone matrix is promising for obtaining bionanocomposite materials suitable for technological applications, such as absorption of pollutants for remediation and conservation of cultural heritage.

Keywords Nanocomposites · Polycaprolactone · Halloysite · Thermal stability · Viscoelastic properties

Introduction

In recent decades, biodegradable polymers have attracted growing interest for the design of novel eco-friendly composites to face urgent environmental issues [1, 2]. Polycaprolactone (PCL) is one of the most promising green and fully biodegradable polymers, although it is not produced from renewable raw materials, but derived from the distillation products of crude oil [3]. It is a thermoplastic and semicrystalline polymer belonging to the aliphatic polyester family, whose monomeric unit is ε-caprolactone ($C_6H_{10}O_2$). PCL has a l melting point range of 58–64 °C depending on the degree of crystallization and molecular mass, while the glass transition temperature is ca. − 60 °C. The unique properties of the polymer have made it a popular material for several applications, such as tissue engineering, drug delivery and food packaging [4]. Nevertheless, it should be evidenced that the use of PCL is limited by its low thermal stability and poor mechanical strength [5]. Recent studies have reported that the combination of PCL with different types of fillers may improve its physicochemical properties conferring functional properties to the composite material [6].

Halloysite nanotubes (HNTs) have been recently investigated for the preparation of PCL-based composite with appealing performances [4, 7]. Halloysite is a type of naturally occurring clay mineral with a chemical composition similar to the most common kaolinite, except for the presence of the water molecules (typically two) hosted between the adjacent alumina and silica layers [8]. Due to the rolling of aluminosilicate sheets, halloysite nanotubes possess a unique spiral-like morphology [9]. Halloysite nanotubes are composed by ca. 15 aluminosilicate layers.

✉ Giuseppe Cavallaro
giuseppe.cavallaro@unipa.it

[1] Dipartimento di Fisica e Chimica "E. Segrè", Università degli Studi di Palermo, Viale delle Scienze, Pad. 17, 90128 Palermo, Italy

[2] INAF – Astronomical Observatory "G. S. Vaiana", Piazza del Parlamento, 1, Palermo, Italy

The external surface is composed of siloxane (Si–O–Si) groups, while the inner one consists of a gibbsite-like array of aluminol (Al–OH) groups. The different surface chemistry was exploited for the selective functionalization of halloysite by ionic molecules (surfactants, polymers, proteins) driving to obtain functional nanomaterials suitable for several purposes, including pharmaceutics [10, 11], cosmetics [12] and catalysis [13]. Generally, halloysite possesses a length in the range of 0.2–1.5 μm, while the inner and outer diameters of the tubes are 10–30 and 40–70 nm, respectively. It should be noted that the sizes and the polydispersity of halloysite depend on the extraction site and purification processes [14, 15].

Due to their morphology and surface characteristics, halloysite nanotubes were successfully employed as catalytic supports [16–18] and reinforcement nanofillers for polymeric matrix [19–23]. Remarkably, halloysite is a biocompatible and non-toxic nanomaterial as evidenced by both in vitro and in vivo tests [24–26]. On this basis, HNTs can be used for biomedical applications, such as tissue engineering [27, 28] and controlled delivery of active molecules [29–33].

Literature reports that the addition of HNTs may confer enhanced mechanical properties, thermal stability and anti-flammability characteristics to polymer matrices likely polyethylene, polypropylene, nylons, epoxy resin and rubbers with appealing perspective in several applications [7]**.** As reported in recent literature [34, 35], the HNTs-mediated modification of PCLs affects the properties of the bionanocomposites.

The combination of halloysite and PCL was explored to obtain composite materials for decontamination purposes, such as the removal of pollutants from soil and water [36, 37]. On the other hand, the efficiency of PCL/HNTs composites for the absorption of pollutants in gas phase was not completely investigated [38].

Here, we investigated PCL/HNTs composites prepared by melt blending. The halloysite content was changed up to 60 mass%, which represents the largest HNTs content to obtain homogeneous materials. Then, we studied the influence of halloysite on the thermal and mechanical properties of PCL by using several thermal analysis methods, including thermogravimetry, differential scanning calorimetry and dynamic mechanical analysis. These techniques are suitable to investigate inorganic [39–41] and organic [42, 43] materials as well as composites [44–47]. Additionally, we examined the influence of HNTs on the PCL crystallization behavior by both differential scanning calorimetry and XRD spectroscopy. Within cultural heritage applications, this study represents a starting step to develop green composite materials with thermomechanical properties suitable as sorbents of gaseous pollutants allowing the preservation of artworks.

Experimental

Materials

Halloysite nanotubes (HNTs) are from I-Minerals Inc (USA, Idaho, USA). Polycaprolactone (PCL, average molecular mass of ca. 14,000 g mol^{-1}, melting point: about 60°, density: 1.146 g mL^{-1} at 25 °C) is a Sigma-Aldrich product (St. Louis, MO, USA), in the form of flakes. Both products were used without any purification.

Preparation of PCL/HNTs nanocomposites

PCL/HNTs composites were prepared by melt blending procedure. To this purpose, different concentrations of HNT powder were physically mixed with PCL in molten state (Table 1) within a ceramic mortar. The blends were heated repeatedly inside the stove (at a temperature of ca. 80 °C for 1 h) to melt the polymer and manually stirred for 15 min until the nanotubes were fully dispersed within the PCL matrix.

Finally, the hybrid materials were stored in a desiccator at 25 °C. These materials last at least for 12 months. We prepared nanocomposites at variable composition with HNTs content ranging from 5 to 60 mass%. Table 1 reports the amounts of both components (PCL and HNTs) mixed for the preparation of the nanocomposites.

Figure 1 shows scanning electron microscopy (SEM) images of pristine PCL and PCL filled with 60 mass% HNTs. We observed that the presence of halloysite induces an increase of the surface roughness proving the HNTs embedding within the polymer matrix.

Methods

Thermogravimetric analyses (TGA) were carried out by using Q5000 IR instrument (TA Instruments, Milan, Italy) under nitrogen flows of 25 and 10 cm^3 min^{-1} for the sample and the balance, respectively. The samples (ca. 5 mg) were heated from 20 to 800 °C using a scanning rate of 20 °C min^{-1}. The temperature calibration was carried out by

Table 1 Amounts of PCL and HNTs used for the preparation of the composites

Sample	Mass PCL/g	Mass HNTs/g
PCL	5.00	0
PCL/HNTs 5 mass%	5.00	0.26
PCL/HNTs 15 mass%	5.00	0.88
PCL/HNTs 35 mass%	5.00	2.69
PCL/HNTs 50 mass%	5.00	5.00
PCL/HNTs 60 mass%	5.00	7.5

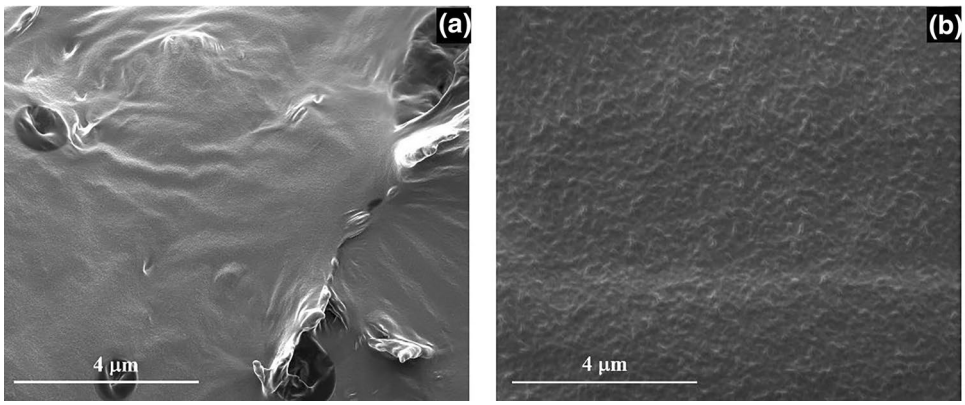

Fig. 1 SEM images of PCL and PCL/HNTs nanocomposite with halloysite content of 60 mass%

means of the Curie temperatures of standards (nickel, cobalt and their alloys) [48].

Micro differential scanning calorimetry (μ-DSC) was conducted by micro-DSC III 106 (Setaram, Lyon, France) under nitrogen atmosphere. Samples of ca. 5 mg were heated from 25 to 80 °C using scanning rate of 1 °C min^{-1}.

The analysis of the μ-DSC peak allowed us to determine the temperature (T_m) and the enthalpy (ΔH_m) of PCL melting process. Specifically, T_m was estimated from the temperature at the minimum of the peak. On the other hand, ΔH_m was calculated by integrating the area under the μ -DSC peak.

Differential scanning calorimetry (DSC) experiments were conducted to investigate the influence of HNTs on the kinetics of PCL crystallization process. DSC measurements were performed by using DSC 250 instrument (TA Instruments, Milan, Italy) under nitrogen atmosphere. Samples of ca. 5 mg were heated at 90 °C and kept for 5 min to eliminate any previous thermal history; then, the samples were cooled down to 0 °C using different scanning rates 5, 10, 15, 20 and 25 °C min^{-1}).

X-ray diffraction (XRD) analyses were also employed to determine the crystallinity degree of PCL/HNT composites, using a Rigaku (MiniFlex, Tokyo, Japan) diffractometer with monochromatic Cu Kα radiation source, including a nickel filter. The patterns were recorded in the range 2–70° with a rate of 20° min^{-1} and a step of 0.02°. The voltage was 40 kV, and the current was 15 mA. The samples were prepared by melting the composites and forming tablets of appropriate size to fit the instrument's sample stage.

Dynamic mechanical analysis (DMA) was performed by DMA Q800 (TA Instruments, Milan, Italy). The experiments were conducted in the oscillatory regime by using a shear sandwich clamp on samples with a surface of 1 cm^2 and a thickness comprised between 0.4 and 1.4 mm. We studied the effect of the temperature on the storage and loss moduli of PCL-based materials by heating up the samples from 30 to 80 °C with a scanning rate of 2 °C min^{-1}. As reported elsewhere for polymer/HNTs composites [45], the oscillation frequency and the applied strain were set at 1 Hz and 0.5%, respectively.

Scanning electron microscopy (SEM) analyses were performed by a Desktop SEM Phenom PRO X PHENOM microscope using a magnification range of 160 × to 350.000 × and a voltage range between 4.8 and 20.5 kV. Each sample was preliminarily coated with a 3 nm thick layer of gold to prevent charging effects under the electron beam.

Results and discussion

Thermal stability of PCL/HNTs nanocomposites

The effect of HNTs addition on the PCL thermal stability was investigated by thermogravimetric measurements. Figure 2 shows the thermogravimetric (TG) and differential thermogravimetric (DTG) curves of native PCL and PCL/HNTs composites at variable composition. The thermogravimetric curve for the nanocomposite with the largest HNTs content (60 mass%) is presented in Supporting Information.

As shown in Fig. 2, we detected an increase of the residual matter at the highest investigated temperature (800 °C) after the addition of halloysite within the PCL matrix. This effect is related to the inorganic nature of halloysite, which is thermally more resistant at high temperatures respect to PCL that is completely degraded at 600 °C.

In Table 2, the MR_{800} values for all samples are reported. Clearly, we estimated that MR_{800} is proportional to the HNT content of the composites.

TG curves of native HNTs (see Supporting Information) showed two main stages of mass loss. The initial mass loss up to ca. 150 °C is due to the release of water molecules physically adsorbed onto the HNTs, while the mass loss occurring at higher temperature (in the range between ca. 400 and 600 °C) is related to interlayer water molecules typical of the halloysite clay structure [11, 49]. As concerns pristine PCL and PCL/HNTs nanocomposites, the

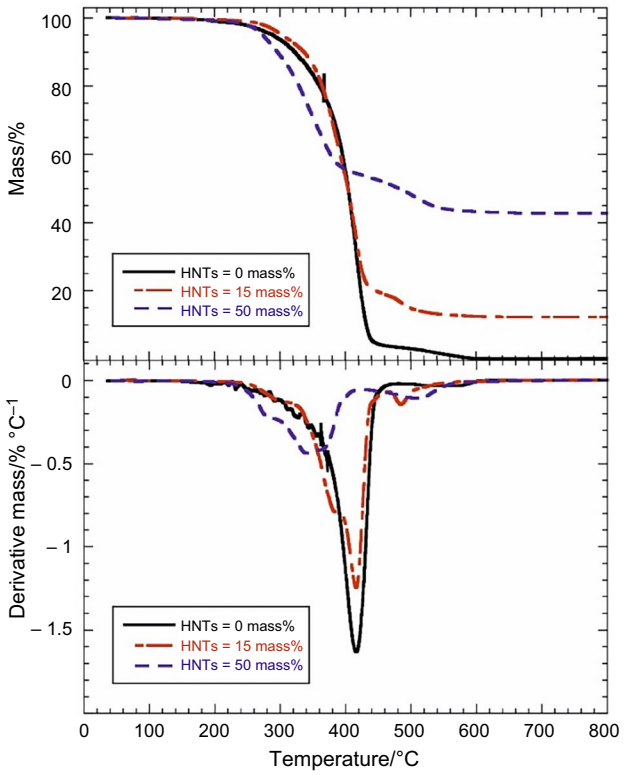

Fig. 2 Thermogravimetric (top) and differential thermogravimetric (bottom) curves of native PCL and PCL/HNTs nanocomposites with halloysite contents of 15 and 50 mass%

Table 2 Residual mass at 800 °C for PCL, HNTs and PCL/HNTs nanocomposites with variable composition

Sample	MR_{800}/ mass%
PCL	0
PCL/HNTs 5 mass%	4.01
PCL/HNTs 15 mass%	12.22
PCL/HNTs 35 mass%	29.85
PCL/HNTs 50 mass%	42.75
PCL/HNTs 60 mass%	50.83
HNTs	84.15

thermogravimetric curves showed the main mass loss in the range between ca. 200 and 420 °C due to the thermal decomposition of the polymer. Accordingly, we estimated the PCL thermal stability by the analysis of the thermogravimetric data within the mentioned degradation interval. Specifically, we calculated the PCL degradation temperature from the minima of the DTG peaks. The obtained results (Table 3) evidenced that the effect of HNTs on the polymer degradation temperature depends on the halloysite concentration.

Table 3 PCL degradation temperatures obtained from the minima of the DTG peaks in the range 200–420 °C and temperatures at 5 and 50% mass losses

Halloysite content/mass%	PCL degradation temperature/°C	$T_{ML5\%}$ /°C	$T_{ML50\%}$ /°C
0	416	289	405
5	412	291	399
15	417	303	404
35	397	284	394
50	341	274	482
60	300	272	757

In particular, we detected that the thermal stability of the polymer is not significantly affected for HNTs ≤ 15 mass%, while further addition of halloysite induced a relevant decrease of the PCL degradation temperature. According to the literature [21], the reduction of the polymer thermal stability could be attributed to the formation of HNT clusters within the polymeric matrix promoting the phase separation in the nanocomposite materials. Namely, we can hypothesize that the percolation threshold for the HNTs aggregation was achieved and the specific interactions between the nanotubes are predominant compared to the polymer/halloysite interactions. It should be noted that the DTG curves of the nanocomposites exhibited a broad peak centered at ca. 500 °C due to the removal of the interlayer water molecules of halloysite. The thermal stability of PCL/HNTs nanocomposites was evaluated also by the determination of the temperatures at 5 and 50% mass losses ($T_{ML5\%}$ and $T_{ML5\%}$) from the quantitative analysis of TG curves. The obtained results are reported in Table 3. According to the previous considerations, both $T_{ML5\%}$ and $T_{ML50\%}$ are significantly decreased for HNTs > 15%. It should be noted that $T_{ML50\%}$ is much higher for the sample with HNTs = 60% because the percentage of inorganic filler is predominant to the organic polymer.

Effect of halloysite addition on PCL melting

DSC experiments were carried out on PCL/HNTs nanocomposites to investigate the effect of halloysite addition on the polymer melting process. Figure 3 shows the μ-DSC curves for native PCL and nanocomposites with variable HNTs contents (15 and 50 mass%), while Supporting Information shows the μ-DSC curve for the nanocomposite with the largest HNTs concentration (60 mass%). As a general observation, we detected an endothermic signal that reflects the melting of the polymer.

The analysis of the DSC peak allowed us to determine the temperature (T_m) and the enthalpy (ΔH_m) of PCL melting process. Specifically, T_m was estimated from the temperature at the minimum, while ΔH_m was calculated

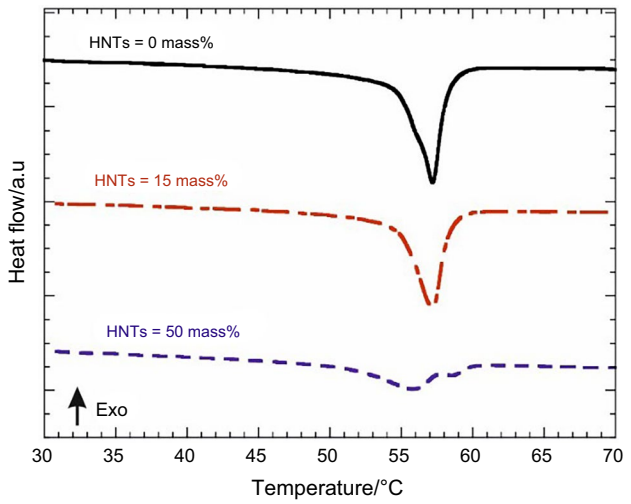

Fig. 3 μ -DSC curves (determined by heating ramp at 1 °C min^{-1}) of native PCL and PCL/HNTs nanocomposites with halloysite concentrations of 15 and 50 mass%

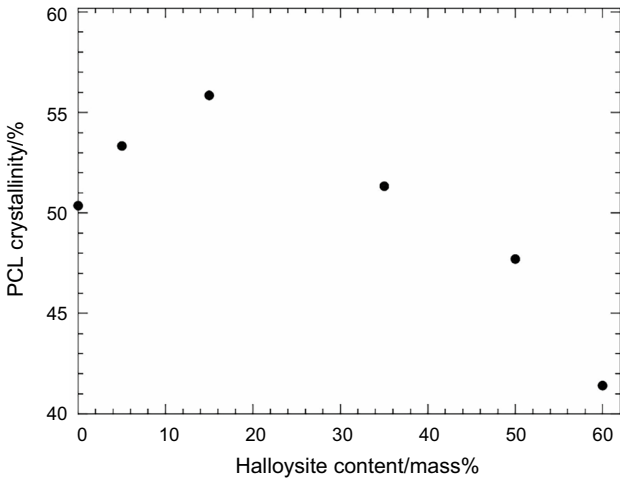

Fig. 4 Dependence of PCL crystallinity on the halloysite content of the nanocomposites

from the integration of peak. Table 2 collects T_m and ΔH_m values for native PCL and PCL/HNTs nanocomposites. These parameters for native PCL and PCL/HNTs nanocomposites are reported in Table 4. It should be noted that the enthalpy data are expressed as Joule per gram of PCL.

We observed that the PCL melting temperature is slightly affected by halloysite addition within the whole investigated concentrations. Compared to native PCL, the nanocomposites exhibited larger melting enthalpy for HNTs ≤ 15 mass%, while a further addition of halloysite caused a ΔH_m reduction. These results could be interpreted by considering the effect of halloysite on the PCL crystallinity (χ_{PCL}), which was calculated as

$$c_{PCL} = 100\left(\Delta H_m/\Delta H_m^*\right) \quad (1)$$

where ΔH_m^* (135 J g^{-1}) is the melting enthalpy of totally crystalline PCL [50].

Table 4 Temperature and enthalpy of PCL melting for nanocomposites with variable halloysite content

Halloysite content/mass%	Melting temperature/°C	Melting enthalpy/J g_{PCL}^{-1}
0	57.3	68.0
5	57.4	72.0
15	57.1	75.4
35	55.4	69.3
50	55.3	64.4
60	55.0	55.9

Figure 4 shows the dependence of PCL crystallinity on the halloysite concentration of the nanocomposites.

The peculiar effect of halloysite on the PCL crystallinity is strongly affected by the nanofiller concentration of the nanocomposites. We detected that HNTs cause an increase of the PCL crystalline degree within a low filler regime indicating that the clay nanotubes can act as nucleating sites within the polymeric matrix enhancing the crystallization kinetics [51]. Similar results were observed for polylactide filled with layered silicates [52]. In contrast, the nanocomposites with a larger HNTs content (≥ 35 mass%) evidenced a decrease of the PCL crystallinity that could be attributed to the reduction of the mobility of the polymeric chains [51]. It should be noted that literature evidenced that the peculiar effect of halloysite on the PCL crystallinity depends on the specific composition of the nanocomposites as well as their preparation protocol [7, 51]. Contrary to our study, literature reports thermal investigations of PCL/HNTs nanocomposites within a low nanofiller regime. As example, Lee et. al. [7] explored the thermal characteristics of nanocomposites with HNTs content up to 10 mass% highlighting that the addition of halloysite induces a reduction of PCL crystallinity, influence of halloysite.

Effect of halloysite addition on PCL crystallization

DSC experiments under cooling ramps at different scanning rates were performed on native PCL and PCL-based nanocomposites with the smallest (5 mass%) and the largest (60 mass%) halloysite concentrations. As shown in Fig. 5, the PCL crystallization is evidenced by exothermic peaks,

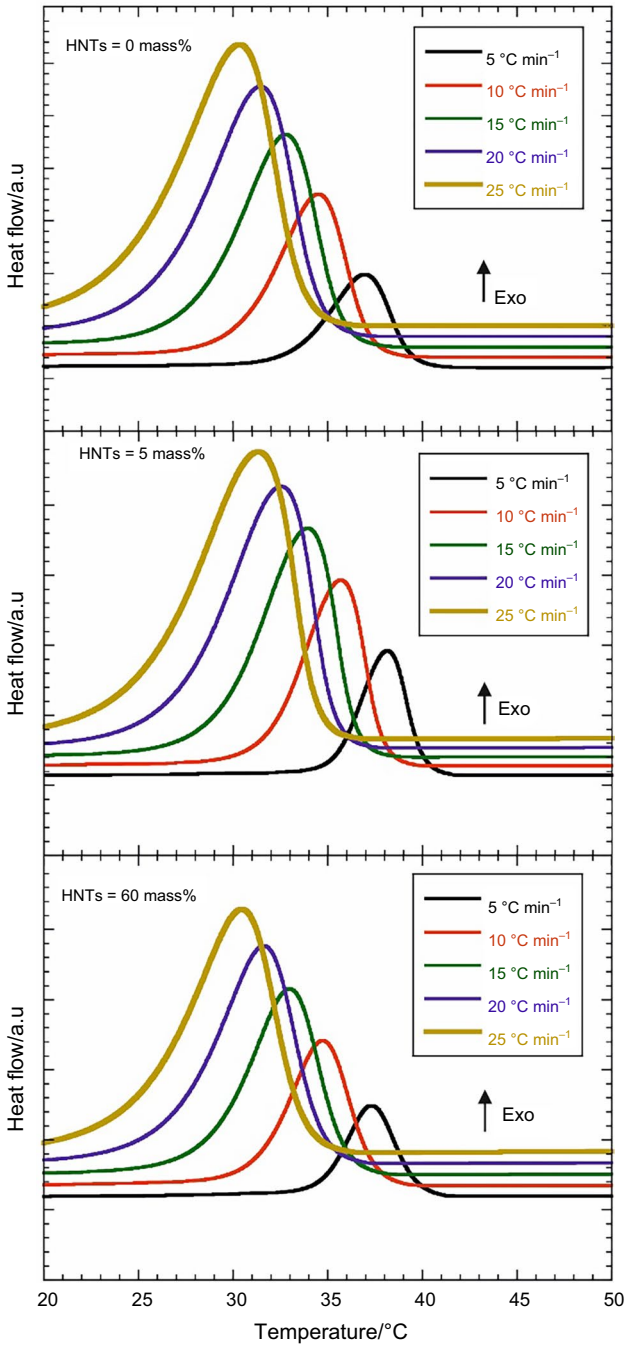

Fig. 5 DSC curves (determined by cooling ramps at five different scanning rates) of native PCL and PCL/HNTs nanocomposites with the lowest (5 mass%) and the highest (60 mass%) halloysite concentrations

which are shifted to lower temperatures by increasing the cooling rate.

As reported for PLA/HNTs nanocomposites [53], the analysis of DSC curves allowed us to estimate the crystallization half-time ($t_{1/2}$), which is the time to achieve 50% relative polymer crystallinity, according to Eq. 2

$$t_{1/2} = (T_0 - T)/b \tag{2}$$

where T_0 is the temperature at which the cooling process begins, and T is the temperature at the maximum peak of the process. β corresponds to the scanning rate used for the analysis. We calculated $t_{1/2}$ values of ca. 51, 45 and 58 s for PCL, PCL/HNT 5 mass% and PCL/HNT 60 mass%, respectively. These results indicated that the addition of small amounts of HNTs enhances the PCL crystallization kinetics, while an opposite effect was observed for the nanocomposite with the largest halloysite content. These observations agree with Fig. 4, which shows that the nanotubes act as nucleating agents for HNTs ≤ 15 mass%, while a further addition of halloysite generates a significant reduction of the polymer crystallinity. A similar correlation between polymer crystallinity and crystallization half-time is reported for PLA/HNTs nanocomposites [53].

Furthermore, the analysis of DSC curves at different cooling rates (Fig. 5) allowed us to determine the crystallization activation energy (E_a) by using the Kissinger method, which can be expressed as

$$d\ln\left(b/T_p^2\right)/d\left(1/T_p\right) = -E_a/R \tag{3}$$

where T_p corresponds to the temperature at crystallization peak, while R is the gas constant.

According to Eq. 3, $\ln(\beta/T_p^2)$ vs $1/T_p$ (Kissinger plots) should be described by linear functions with a slope dependent on the activation energy of the crystallization process. Our experimental data (Fig. 6) were successfully fitted by Eq. 3 providing E_a values of − 198, − 201 and − 190 kJ mol^{-1} for PCL, PCL/HNTs 5 mass% and PCL/HNTs 60 mass%, respectively. Based on these results, we can state that the addition of small amounts of halloysite induced an enhancement of PCL crystallization kinetics. Namely, the nanotubes favored the heterogeneous nucleation of the polymer. This finding agrees with increase of PCL crystallinity determined by the analysis of melting process (Fig. 4) as well as with the $t_{1/2}$ reduction. On the other hand, PCL/HNTs nanocomposites with a large halloysite amount (60 mass%) exhibited the highest E_a value, which means that the polymer crystallization process was slowed down compared with pristine PCL. The reduction of the PCL crystallization kinetics could be attributed to the restriction of the PCL chains mobility generating a decrease of the polymer crystallinity (Fig. 4). Similar results were detected for PCL filled with bioactive glass powders [54] and PLA nanofibrils [55].

The effect of HNT content on the crystallization of PCL was further investigated by X-ray diffraction. The X-ray patterns of pure PCL and HNTs and composites with halloysite concentrations of 5 and 60 mass% are shown in Fig. 7.

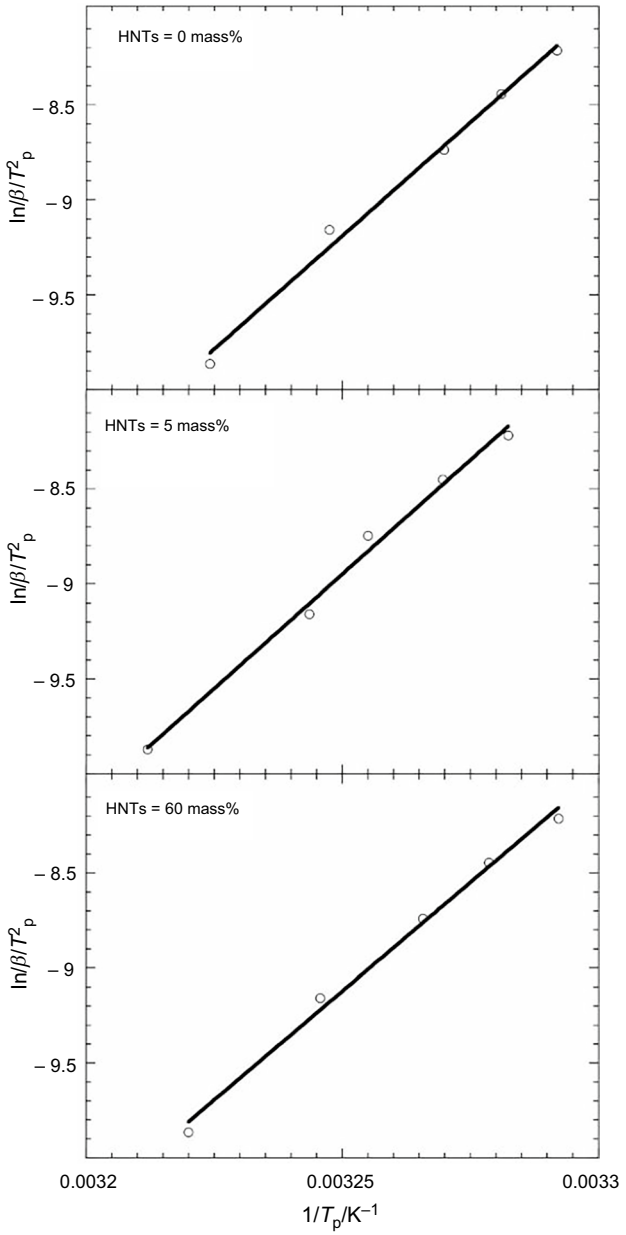

Fig. 6 Kissinger plots for PCL and PCL/HNTs nanocomposites with filler concentrations of 5 and 60 mass%

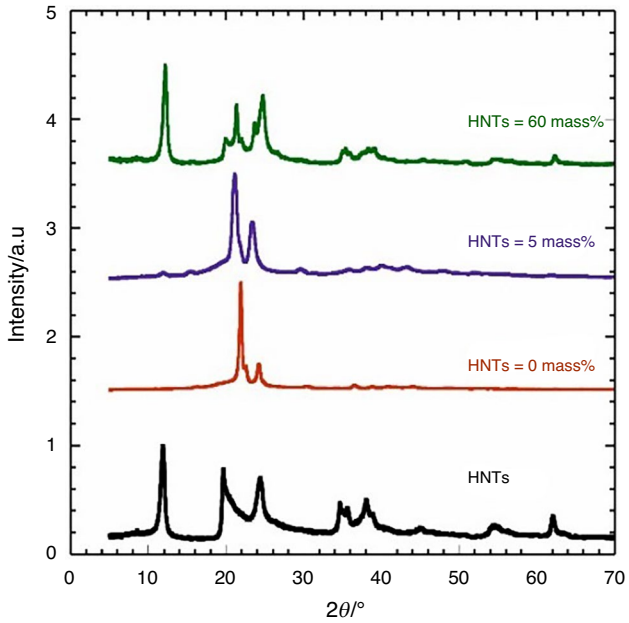

Fig. 7 XRD patterns of pure HNTs and PCL and PCL/HNT composites

PCL showed two sharp peaks at 2θ = 21.9° and 24.2° which are related to (1 1 0) and (2 0 0) diffraction planes, respectively [56]. Moreover, there was a relatively weak peak positioned at 2θ = 16°. These peaks are characteristic of PCL polymer and indicate its semicrystalline nature [56]. Three typical XRD peaks for HNT appeared at 2θ = 11.9°, 19.40° and 24° according to the reflection planes (001), (020) and (002) [15]. The presence of (002) reflection peak at 2θ = 24° and the absence of a peak at 2θ = 8.76° indicate the dehydrated state of HNTs [57]. The diffractogram of the sample with 5% HNT revealed a profile similar to that of the neat PCL. Only a few HNT peaks were distinguishable due to the low proportion of HNT in the matrix. At high filler content (60 mass%), peaks of HNT could be readily observed. The XRD diffractograms showed that as the HNT concentration increased, the intensity of the PCL peaks decreased, while the intensity of the HNT peaks increased. No significant shifts of the position of the diffraction peak related to (110) and (200) planes in PCL were observed in the XRD patterns when HNT was incorporated into the polymer matrix. Consequently, the interplanar spacing of both planes almost remained unchanged with HNTs contents of 5 and 60 mass%, according to the Bragg law. It should be noted that, with the addition of the HNTs, the peaks of PCL and HNT overlapped in the XRD diffractograms, making it not possible to determine quantitatively the degree of crystallinity of the polymer.

Viscoelastic properties of PCL/HNTs nanocomposites

Viscoelastic properties of PCL/HNTs composites at variable temperatures were studied by DMA experiments performed during a heating ramp. As examples, Fig. 8 shows the dependence of tan (δ) on the temperature for native PCL and PCL/HNTs nanocomposites with halloysite contents of 15 and 35 mass%. It should be noted that tan (δ) represents the ratio between the loss (G'') and the storage (G') moduli. DMA data for the nanocomposite with the largest HNTs amount (60 mass%) are reported in Supporting Information.

As shown in Table 5, the addition of halloysite generated a decrease of tan (δ) at 30 °C highlighting that the

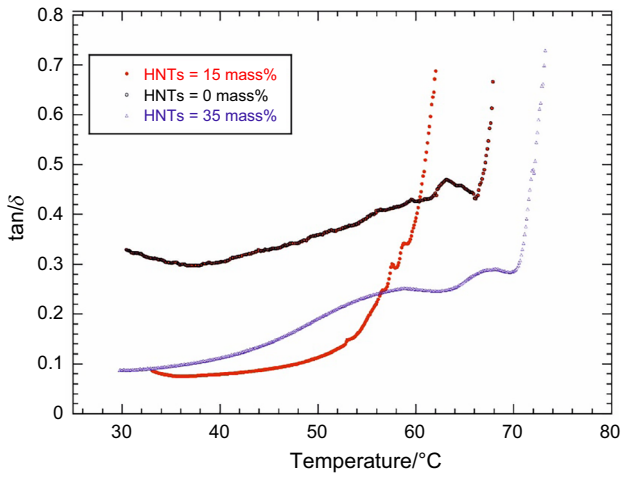

Fig. 8 Tan (δ) as a function of the temperature for PCL/HNTs at variable halloysite concentration

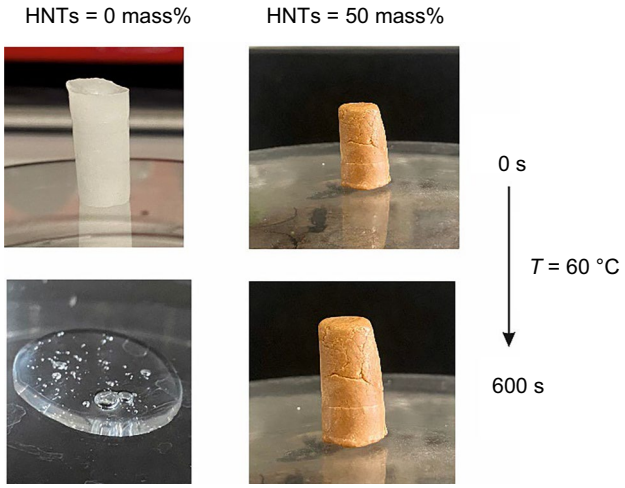

Fig. 9 Photos of cylinders (diameter of ca. 0.5 cm) based on PCL and PCL/HNTs composite with filler content of 50 mass%. The samples were kept at 60 °C for 600 s. The brownish color of PCL filled with HNTs is due to the presence of iron impurities in the halloysite sample

Table 5 Tan (δ) at 25 °C for PCL-based nanocomposites with variable HNTs contents

Halloysite content/ mass%	tan(δ) at 30 °C
0	0.276
5	0.067
15	0.081
35	0.092
50	0.011
60	0.013

nanocomposites possess an improved stored energy capacity with respect to native PCL.

Regarding the viscoelastic response to temperature variations, we observed a sharp tan (δ) increase in the interval between ca. 50 and 70 °C for all the investigated materials. This change reflects an enhancement of the viscous component of the PCL-based materials. Interestingly, we observed that the effect of HNTs on the tan (δ) versus temperature trend is dependent on the specific halloysite concentration of the PCL-based nanocomposites. For HNTs ≤ 15 mass%, the tan (δ) enhancement is shifted to lower temperatures compared to native PCL, while an opposite effect was observed for larger halloysite concentrations. The latter indicates that the elastic properties are preserved at higher temperatures for PCL-based nanocomposites with high filler contents. Namely, the addition of large amounts of HNTs preserves the energy storage capacity of PCL over a wide temperature range. This finding cannot be ascribed to the effects of HNTs on the PCL melting temperature in agreement with DSC results (Table 4). We can hypothesize that the clay nanotubes can create an inorganic skeleton within the polymeric matrix preserving the mechanical behavior of a solid-like material in a larger temperature range. This hypothesis was confirmed by macroscopic experiments (Fig. 9), which showed that native PCL kept at 60 °C (above the melting temperature) for 600 s loses completely its shape, while the composite with HNTs = 50 mass% did not evidence the collapse of its structure. Similar findings were detected for beeswax filled with halloysite clay nanotubes [45].

Conclusions

We successfully prepared nanocomposites based on polycaprolactone (PCL) and halloysite clay nanotubes (HNTs) by using the melt blending procedures. The obtained materials were characterized by thermal analysis techniques (thermogravimetry, differential scanning calorimetry and dynamic mechanical analysis) to investigate the effect of the HNTs concentration on the thermal properties and viscoelastic behavior of PCL. Within a low filler regime (HNTs ≤ 15 mass%), we observed that the degradation temperature is not altered by the halloysite addition. In contrast, the PCL thermal stability was significantly decreases for halloysite contents ≥ 35 mass%, which could be considered as the percolation threshold for the HNTs aggregation. Interestingly, differential scanning calorimetry evidenced that halloysite nanotubes (≤ 15 mass%) can act as nucleating sites for the PCL crystallization, while a reduction of the polymer crystallinity was detected for nanocomposites containing larger HNTs amounts. According to these TGA and DSC results, we observed that the viscoelastic properties of PCL/HNTs nanocomposites are strongly dependent by their composition. We observed that large amounts of HNTs preserve the energy storage capacity of PCL over a wide temperature range compared to native polymers. This finding can be attributed to the formation of an inorganic skeleton based on HNTs within the polymeric

matrix that can extend the mechanical behavior of a solid-like material in a wider temperature range. In conclusion, we can state that PCL filled with a very large HNTs content (> 15%) might be promising as absorbent materials with thermomechanical resistance useful for applications within cultural heritage.

Supplementary Information The online version contains supplementary material available at https://doi.org/10.1007/s10973-025-14178-9.

Acknowledgements The work was financially supported by the University of Palermo, FFR 2024 and European Union—Next Generation EU (PRIN 2022 PNRR—NANOEURO project—Cod. B53D23025300001). This study has been carried out in the context of the SpecoLab project (https://openaccess.inaf.it/handle/20.500.12386/31362) to contrast the presence of pollutants in museum historical showcases.

Funding Open access funding provided by Università degli Studi di Palermo within the CRUI-CARE Agreement. Ministero dell'Istruzione, dell'Università e della Ricerca, PRIN 2022 PNRR—NANOEURO project—Cod. B53D23025300001, Giuseppe Cavallaro

References

1. Lagaron JM, Lopez-Rubio A. Nanotechnology for bioplastics: opportunities, challenges and strategies. Agri-Food Nano Appl Ensuring Soc Benefits. 2011;22:611–7.
2. Yang Y, Haurie L, Wang D-Y. Bio-based materials for fire-retardant application in construction products: a review. J Therm Anal Calorim. 2022;147:6563–82.
3. Phillipson K, Jenkins MJ, Hay JN. The ageing of poly (ε-caprolactone). Polym Int. 2015;64:1695–705.
4. Terzopoulou Z, Papageorgiou DG, Papageorgiou GZ, Bikiaris DN. Effect of surface functionalization of halloysite nanotubes on synthesis and thermal properties of poly(ε-caprolactone). J Mater Sci. 2018;53:6519–41.
5. Rydz J, Sikorska W, Kyulavska M, Christova D. Polyester-based (bio) degradable polymers as environmentally friendly materials for sustainable development. Int J Mol Sci. 2014;16:564–96.
6. Mohamed RM, Yusoh K. A review on the recent research of polycaprolactone (PCL). Adv Mater Res. 2015;1134:249–55.
7. Lee K-S, Chang Y-W. Thermal, mechanical, and rheological properties of poly (ε-caprolactone)/halloysite nanotube nanocomposites. J Appl Polym Sci. 2013;128:2807–16.
8. Wong LW, Pasbakhsh P, Arabi AM, Keeling J, Tan JBL. Halloysite nanotubes from various geological deposits: new insights to acid etching and their impacts on products' characteristics. J Environ Chem Eng. 2021;9:106235.
9. Lisuzzo L, Guercio L, Cavallaro G, Duca D, Ferrante F. Halloysite clay nanotubes for catalytic conversion of biomass: synergy between computational modeling and experimental studies. ACS Catal. 2024;14:18167–203.
10. Feng Y, He Y, Lin X, Xie M, Liu M, Lvov Y. Assembly of clay nanotubes on cotton fibers mediated by biopolymer for robust and high-performance hemostatic dressing. Adv Healthc Mater. 2023;12:2202265.
11. Lisuzzo L, Cavallaro G, Milioto S, Lazzara G. Coating of silk sutures by Halloysite/wax Pickering emulsions for controlled delivery of eosin. Appl Clay Sci. 2024;247:107217.
12. Cavallaro G, Caruso MR, Milioto S, Fakhrullin R, Lazzara G. Keratin/alginate hybrid hydrogels filled with halloysite clay nanotubes for protective treatment of human hair. Int J Biol Macromol. 2022;222:228–38.
13. Lisuzzo L, Cavallaro G, Milioto S, Lazzara G. Halloysite nanotubes as nanoreactors for heterogeneous micellar catalysis. J Colloid Int Sci. 2022;608:424–34.
14. Maria Calvino M, Cavallaro G, Pasbakhsh P, Lazzara G, Milioto S. Hydrogel based on patch halloysite nanotubes: a rheological investigation. J Mol Liq. 2024;394:123721.
15. Cavallaro G, Chiappisi L, Pasbakhsh P, Gradzielski M, Lazzara G. A structural comparison of halloysite nanotubes of different origin by small-angle neutron scattering (SANS) and electric birefringence. Appl Clay Sci. 2018;160:71–80.
16. Sadjadi S, Abedian-Dehaghani N, Heravi MM, Zhong X, Yuan P, Duran J, et al. Clay-supported acidic ionic liquid as an efficient catalyst for conversion of carbohydrates to 5-hydroxymethylfurfural. J Mol Liq. 2023;382:121847.
17. Liu Y, Guan H, Zhang J, Zhao Y, Yang J-H, Zhang B. Polydopamine-coated halloysite nanotubes supported AgPd nanoalloy: an efficient catalyst for hydrolysis of ammonia borane. Int J Hydrog Energy. 2018;43:2754–62.
18. Liu Y, Zhang J, Guan H, Zhao Y, Yang J-H, Zhang B. Preparation of bimetallic Cu-Co nanocatalysts on poly (diallyldimethylammonium chloride) functionalized halloysite nanotubes for hydrolytic dehydrogenation of ammonia borane. Appl Surf Sci. 2018;427:106–13.
19. Bugatti V, Sorrentino A, Gorrasi G. Encapsulation of lysozyme into halloysite nanotubes and dispersion in PLA: structural and physical properties and controlled release analysis. Eur Polym J. 2017;93:495–506.
20. Boccalon E, Sassi P, Pioppi L, Ricci A, Marinozzi M, Gorrasi G, et al. Onion skin extract immobilized on Halloysite-layered double hydroxide filler as active pH indicator for food packaging. Appl Clay Sci. 2022;227:106592.
21. Lisuzzo L, Cavallaro G, Milioto S, Lazzara G. Effects of halloysite content on the thermo-mechanical performances of composite bioplastics. Appl Clay Sci. 2020;185:105416.
22. Kalathil MR, Santoshi RB, Rasana N, Jayanarayanan K. Non-isothermal crystallization kinetics of halloysite nanotube/short glass fibre-reinforced polypropylene composites. J Therm Anal Calorim. 2023;148:11765–81.
23. Petková M, Ryba J, Hrabovská V, Ujhelyiová A, Hricová M. The crystallization of polypropylene/halloysite fibers. J Therm Anal Calorim. 2019;136:1093–101.
24. Kryuchkova M, Danilushkina A, Lvov Y, Fakhrullin R. Evaluation of toxicity of nanoclays and graphene oxide in vivo: a paramecium caudatum study. Environ Sci Nano. 2016;3:442–52.
25. Rozhina E, Panchal A, Akhatova F, Lvov Y, Fakhrullin R. Cytocompatibility and cellular uptake of alkylsilane-modified hydrophobic halloysite nanotubes. Appl Clay Sci. 2020;185:105371.
26. Xue W, Jiachun G, Gui Zongxiang Hu, Xiaolong TX. Halloysite nanotubes-induced Al accumulation and oxidative damage in liver of mice after 30-day repeated oral administration. Environ Toxicol. 2018;33:623–30.

27. Naumenko E, Fakhrullin R. Halloysite nanoclay/biopolymers composite materials in tissue engineering. Biotechnol J. 2019;14:1900055.
28. Liu M, Dai L, Shi H, Xiong S, Zhou C. In vitro evaluation of alginate/halloysite nanotube composite scaffolds for tissue engineering. Mater Sci Eng C. 2015;49:700–12.
29. Li R, Zhang Y, Lin Z, Lei Q, Liu Y, Li X, et al. Injectable halloysite-g-chitosan hydrogels as drug carriers to inhibit breast cancer recurrence. Compos Part B Eng. 2021;221:109031.
30. Fizir M, Dramou P, Dahiru NS, Ruya W, Huang T, He H. Halloysite nanotubes in analytical sciences and in drug delivery: a review. Microchim Acta. 2018;185:389.
31. Liu F, Bai L, Zhang H, Song H, Hu L, Wu Y, et al. Smart H_2O_2-responsive drug delivery system made by halloysite nanotubes and carbohydrate polymers. ACS Appl Mater Interfaces. 2017;9:31626–33.
32. Duce C, Porta VD, Bramanti E, Campanella B, Spepi A, Tiné MR. Loading of halloysite nanotubes with BSA, α -Lac and β -Lg: a Fourier transform infrared spectroscopic and thermogravimetric study. Nanotechnology. 2017;28:055706.
33. Spepi A, Duce C, Pedone A, Presti D, Rivera J-G, Ierardi V, et al. Experimental and DFT characterization of halloysite nanotubes loaded with salicylic acid. J Phys Chem C. 2016;120:26759–69.
34. Bulbul YE, Uzunoglu T, Dilsiz N, Yildirim E, Ates H. Investigation of nanomechanical and morphological properties of silane-modified halloysite clay nanotubes reinforced polycaprolactone bio-composite nanofibers by atomic force microscopy. Polym Test. 2020;92:106877.
35. Kaur G, Gupta S, Prakash V, Rodriguez RD, Sheremet E, Mehta SK, et al. A comprehensive review of varied applications of modified halloysite nanocomposites. Nano-Struct Nano-Objects. 2024;39:101230.
36. Yu L, Wang H, Zhang Y, Zhang B, Liu J. Recent advances in halloysite nanotube derived composites for water treatment. Environ Sci Nano. 2016;3:28–44.
37. Kayan GÖ, Kayan A. Polycaprolactone Composites/Blends and Their Applications Especially in Water Treatment. ChemEngineering [Internet]. 2023;7. Available from: https://www.mdpi.com/2305-7084/7/6/104
38. Wal K, Rutkowski P, Stawiński W. Application of clay minerals and their derivatives in adsorption from gaseous phase. Appl Clay Sci. 2021;215:106323.
39. Matejka L, Siler P, Novotny R, Svec J, Masilko J, Koplik J, et al. The thermal analysis of zinc oxide-contaminated Portland cement blended with thiocyanates and determination of their effect on hydration and properties. J Therm Anal Calorim. 2023;148:1321–49.
40. Kuzielová E, Slaný M, Žemlička M, Másilko J, Šiler P, Palou MT. Thermal stability of the phases developed at high-pressure hydrothermal curing of class G cement with different pozzolanic and latent hydraulic additives. J Therm Anal Calorim. 2022;147:9891–902.
41. Švec J, Šiler P, Másilko J, Novotný R, Koplík J, Janča M, et al. Simultaneous thermogravimetric and differential thermal analysis determination of products formed during hydration of blended Portland cement doped with zinc. J Therm Anal Calorim. 2020;142:1749–58.
42. Brusnikina M, Silyukov O, Chislov M, Volkova T, Proshin A, Terekhova I. New water-soluble dosage forms of 1,2,4-thiadiazole derivative on the basis of inclusion complexes with cyclodextrins. J Therm Anal Calorim. 2017;127:1815–24.
43. Kritskiy I, Volkova T, Surov A, Terekhova I. γ-Cyclodextrin-metal organic frameworks as efficient microcontainers for encapsulation of leflunomide and acceleration of its transformation into teriflunomide. Carbohydr Polym. 2019;216:224–30.
44. Volkova TV, Domanina EN, Chislov MV, Proshin AN, Terekhova IV. Polymeric composites of 1,2,4-thiadiazole: solubility, dissolution and permeability assay. J Therm Anal Calorim. 2020;140:2305–15.
45. Cavallaro G, Lazzara G, Milioto S, Parisi F, Sparacino V. Thermal and dynamic mechanical properties of beeswax-halloysite nanocomposites for consolidating waterlogged archaeological woods. Polym Degrad Stab. 2015;120:220–5.
46. Erceg M, Krešić I, Jakić M, Andričić B. Kinetic analysis of poly(ethylene oxide)/lithium montmorillonite nanocomposites. J Therm Anal Calorim. 2017;127:789–97.
47. Jakić M, Vrandečić NS, Erceg M. The influence of poly(ethylene glycol) on thermal properties of poly(vinyl chloride)/poly(ethylene oxide) blends. J Therm Anal Calorim. 2017;127:663–74.
48. Blanco I, Cicala G, Latteri A, Saccullo G, El-Sabbagh AMM, Ziegmann G. Thermal characterization of a series of lignin-based polypropylene blends. J Therm Anal Calorim. 2017;127:147–53.
49. Joussein E, Petit S, Churchman GJ, Theng B, Righi D, Delvaux B. Halloysite clay minerals—a review. Clay Miner. 2005;40:383–426.
50. Wang S, Yaszemski MJ, Gruetzmacher JA, Lu L. Photocrosslinked poly (ε-caprolactone fumarate) networks: roles of crystallinity and crosslinking density in determining mechanical properties. Polymer. 2008;49:5692–9.
51. Di Maio E, Iannace S, Sorrentino L, Nicolais L. Isothermal crystallization in PCL/clay nanocomposites investigated with thermal and rheometric methods. Polymer. 2004;45:8893–900.
52. Nam JY, Sinha Ray S, Okamoto M. Crystallization behavior and morphology of biodegradable polylactide/layered silicate nanocomposite. Macromolecules. 2003;36:7126–31.
53. Biazin GG, Beatrice CAG, de Thiago A, Augusto JM, Costa LC. Quiescent and shear-induced non-isothermal crystallization kinetics of PLA/HNT nanocomposites. J Therm Anal Calorimetry. 2023;148(23):13463–85. https://doi.org/10.1007/s10973-023-12648-6.
54. Pires LSO, Fernandes MHFV, de Oliveira JMM. Crystallization kinetics of PCL and PCL–glass composites for additive manufacturing. J Therm Anal Calorim. 2018;134:2115–25.
55. Qiao Y, Li Q, Jalali A, Yang J, Wang X, Zhao N, et al. In-situ microfibrillated Poly(ε-caprolactone)/ Poly(lactic acid) composites with enhanced rheological properties, crystallization kinetics and foaming ability. Compos Part B Eng. 2021;208:108594.
56. Baji A, Wong S-C, Liu T, Li T, Srivatsan TS. Morphological and X-ray diffraction studies of crystalline hydroxyapatite-reinforced polycaprolactone. J Biomed Mater Res B Appl Biomater. 2007;81B:343–50.
57. Dong Y, Marshall J, Haroosh HJ, Mohammadzadehmoghadam S, Liu D, Qi X, et al. Polylactic acid (PLA)/halloysite nanotube (HNT) composite mats: influence of HNT content and modification. Compos Part Appl Sci Manuf. 2015;76:28–36.